Journal of Intelligent and Connected Vehicles
2023, **6**(1): 46–63
https://doi.org/10.26599/JICV.2023.9210004

Research Article

Human-like lane-changing trajectory planning algorithm for human–machine conflict mitigation

Changhua Dai[1], Changfu Zong[1], Dong Zhang[2,✉], Gang Li[3], Kaku Chuyo[4], Hongyu Zheng[1], Fei Gao[1]

[1]*State Key Laboratory of Automotive Simulation and Control, Jilin University, Changchun 130022, China*
[2]*Department of Mechanical and Aerospace Engineering, Brunel University London, UB8 3PH, UK*
[3]*College of Automobile and Traffic Engineering, Liaoning University of Technology, Jinzhou 121000, China*
[4]*Jiangsu Chaoli Electric Co., Ltd., Danyang 212300, China*

Received: December 9, 2022; Revised: January 13, 2023; Accepted: February 6, 2023

ABSTRACT: The purpose of this paper is to alleviate the potential safety problems associated with the human driver and the automatic system competing for the right of way due to different objectives by mitigating the human-machine conflict phenomenon in human-machine shared driving (HMSD) technology from the automation system. Firstly, a basic lane-changing trajectory algorithm based on the quintic polynomial in the Frenet coordinate system is developed. Then, in order to make the planned trajectory close to human behavior, naturalistic driving data is collected, based on which some lane-changing performance features are selected and analyzed. There are three aspects have been taken into consideration for the human-like lane-changing trajectory: vehicle dynamic stability performance, driving cost optimization, and collision avoidance. Finally, the HMSD experiments are conducted with the driving simulator to test the potential of the human-like lane-changing trajectory planning algorithm. The results demonstrate that the lane-changing trajectory planning algorithm with the highest degree of personalization is highly consistent with human driver behavior and consequently would potentially mitigate the human-machine conflict with the HMSD application. Furthermore, it could be further employed as an empirical trajectory prediction result. The algorithm employs the distribution state of the historical trajectory for human-like processing, simplifying the operational process and ensuring the credibility, integrity, and interpretability of the results. Moreover, in terms of optimization processing, the form of optimization search followed by collision avoidance detection is adopted to in principle reduce the calculation difficulty. Additionally, a new convex polygon collision detection method, namely the vertex embedding method, is proposed for collision avoidance detection.

KEYWORDS: human–machine conflict, human–machine shared driving (HMSD), human-like lane-changing trajectory planning, collision avoidance, trajectory prediction

1 Introduction

The development of automotive intelligence is an important direction and research hotspot in the 21st century. Its technical architecture includes environmental perception (Cao et al., 2015; Yan et al., 2018), short-term prediction (Qi et al., 2017), behavioral decision-making (Tan et al., 2019), trajectory planning (Zhou et al., 2019a, 2019b; Peng et al., 2020), and path tracking (Xu and Peng, 2019; Xu et al., 2020). According to SAE's classification criteria for intelligent vehicle, human-machine interaction technology is at the L1–L3 level of intelligent automobile development (Russell et al., 2016), which includes multi-level technical functions (Yuan and Zhang, 2020; Kim et al., 2016). Previously, research on human-machine shared driving (HMSD) focused on the control layer (Naand Cole, 2013; Li et al., 2019). Today, researchers are increasingly concerned about human-machine conflicts due to inconsistent human-machine tracking objectives (Huang et al., 2021). Working with the automatic system of trajectory planning that does not consider the driving habits of human drivers may reduce the trust and acceptance of the automated system by human drivers, who compete with the automated system for the right of way.

There are five main categories of existing lane-changing trajectory planning methods: graph search-based algorithm, sampling-based algorithm, interpolating curve algorithm, numerical optimization algorithm, and mechanism model-based algorithm (Zheng et al., 2019). With the objective of improving human driver acceptance and satisfaction with lane-changing, a few researchers have proposed human-like lane-changing trajectory planning in which the lane-changing habits of human drivers are gradually taken into account. For example, Ali et al. (2021) proposed to capture the driver's driving behaviour in a driving simulator and investigated the factors influencing forced and free lane-changing. A human-like lane-changing trajectory planning algorithm based on cubic polynomial interpolation was proposed by Zhang et al. (2019). Wang et al. (2016) proposed a lane-changing trajectory planning model based on linear offset and sine function to balance driver comfort and vehicle dynamics. Zhu et al. (2018) proposed a sine-wave lane-changing model, which integrates driver behavior recognition strategy to implement a human-like lane-changing assistant system. He et al. (2018) proposed a trajectory planning method based on quintic polynomial by learning from human driving data.

✉ Corresponding author.
E-mail: dong.zhang@brunel.ac.uk

In the above human-like lane-changing trajectory planning research, the basic technical route is data collection to style classification and stylized trajectory planning. With respect to the classification level of the degree of personalization, this technical route presents a lower level of personalization. Although it could reflect the style of human drivers to a certain extent, it shows results in style attributes that fall under the typical segmentation classification method, i.e., a lower level of personalization (Sun, 2020). The individual scenarios belonging to the edge of classification are significantly different from those belonging to the classification center. In addition, Zhang et al. (2021) demonstrated that there are individual scenarios differences in the requirements for autonomous driving. A classified and stylized technical route could not satisfy the unique requirements of all individual scenarios.

In order to improve the level of personalization of autonomy and thus mitigate the potential conflict between the driver and the automatic systems at the planning level, this paper proposes a highly human-like lane-changing trajectory planning algorithm. The logic block diagram of the proposed algorithm is shown in Fig. 1. Firstly, the lane-changing features of human drivers are analyzed with the collection of natural lane-changing data. Then, based on the selected lane-changing features, the quintic polynomial is introduced to generate trajectory clusters based on the minimum fluctuation lane-changing objective. Furthermore, the human-like lane-changing trajectory takes full consideration of the dynamic stability performance of the vehicle, driving cost optimization, and collision avoidance. The main contributions of this paper could be concluded as follows:

1) At the macro level, a quintic polynomial trajectory planning algorithm based on a single independent variable is developed in conjunction with historical lane-changing driving data obtained from human drivers. The lane-changing features and trajectory expressions then can be directly combined. In contrast to machine classification algorithms, it could be adapted to different human drivers with higher accuracy through normal distribution analysis. In the HMSD, it shows great benefits in mitigating human-machine conflict, thus improving the vehicle safety in dangerous situation for potential confrontation.

2) The optimal search algorithm is conducted before the collision avoidance detection, reducing the computation time of the algorithm. In addition, a new convex polygon collision detection method is proposed for collision avoidance detection, namely the vertex embedding method, which demonstrates great efficiency in vehicle collision avoidance in real time using simple geometry theory.

3) In terms of application scenarios, the method could be applied to the field of human driver trajectory prediction because the planned trajectory highly matches the human driver lane-changing trajectory clusters. Therefore, it would be beneficial for the further development of intelligent transportation systems with mixed traffic participants.

This work is organized as follows: Section 2 establishes a lane-changing trajectory algorithm based on the Frenet coordinate system (FCS) with a quintic polynomial. In Section 3, we use the extended driving simulator to collect the lane-changing data of human drivers and analyze the lane-changing features. In Section 4, human-like lane-changing trajectory obtained by stability search, optimal search, and collision avoidance detection. In Section 5, the planning algorithm and the confidence level of lane-changing trajectory with human drivers are verified, and the trajectory tracking co-simulation is implemented in Simulink/CarSim. In Section 6, the planned human-like lane-changing trajectory is employed for the HMSD experiments through a driving simulator. And Section 7 includes the conclusions.

2 FCS-based lane-changing trajectory planning with quintic polynomial

In order to provide a basic lane-changing trajectory algorithm for a human-like lane-changing strategy, this section develops a lane-changing trajectory algorithm based on the longitudinal and lateral quintic polynomials of the FCS (Werling et al., 2012; Zheng et al., 2020).

The geodetic coordinate system (GCS) is used by most existing vehicle positioning equipments (Yang, 2009; Vigue, 1992). In the GCS, due north and due west are taken as coordinate axes. Although the coordinate system is fixed and easy to obtain, it poses an inconvenience to the application of local trajectory planning. This is because the local trajectory planning of non-linear roads involves considering the effect of road curvature on the expression of the trajectory function. The FCS takes the road center line as the abscissa and the normal direction perpendicular to the road center line as the ordinate. The FCS could transform the curve into straight lines, eliminating the above inconvenience.

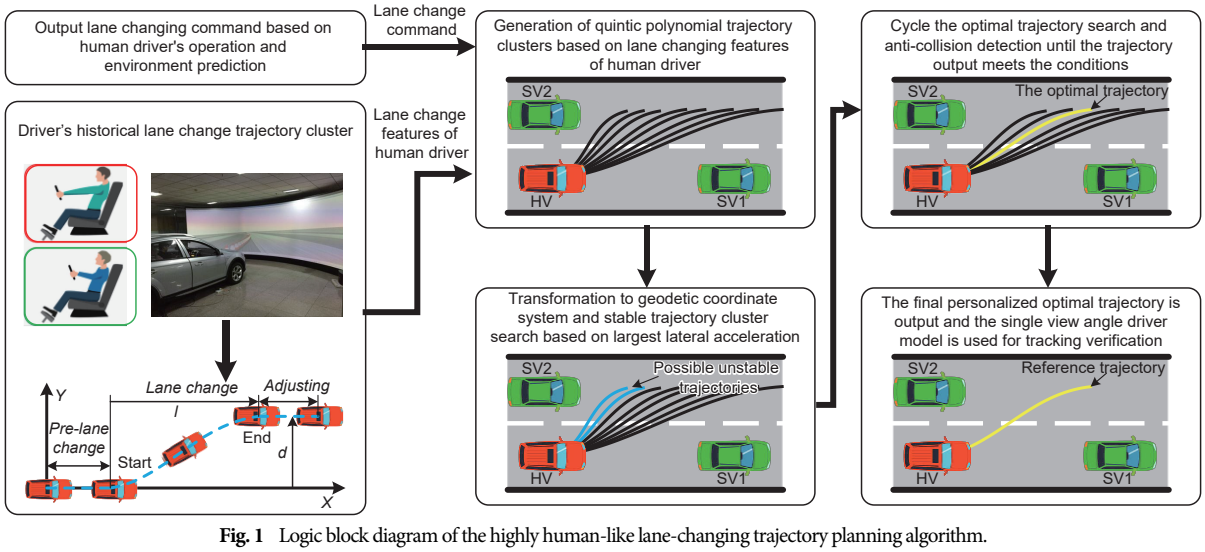

Fig. 1 Logic block diagram of the highly human-like lane-changing trajectory planning algorithm.

清華大学出版社 Tsinghua University Press | IEEE

2.1 Longitudinal derivation in FCS

During the process of lane-changing, the human drivers typically want to minimize the fluctuation of lateral and longitudinal motion as much as possible to guarantee the stability of the moving process. Therefore, longitudinal acceleration is regarded as the fluctuation in longitudinal motion, and the performance indicators are developed to minimize longitudinal fluctuation:

$$\min_{j_s(t)} \int_{t_s}^{t_e} j_s^2(t)\mathrm{d}t \tag{1}$$

s.t.

$$\dot{s}(t) = v_s(t)$$

$$\ddot{s}(t) = \dot{v}_s(t)$$

$$\dot{a}_s(t) = j_s(t)$$

$$s(t_s) = 0, s(t_e) = s_e$$

$$v_s(t_s) = v_{ss}, v_s(t_e) = v_{se}$$

$$a_s(t_s) = a_{ss}, a_s(t_e) = a_{se}$$

where j_s is the longitudinal jerk; s is the longitudinal displacement; s_e is the longitudinal displacement at the end of lane-changing; v_s, v_{ss}, and v_{se} are the longitudinal velocity, the start and end longitudinal velocity of lane-changing, respectively; a_{ss} and a_{se} are the longitudinal acceleration at the start and end of lane-changing, respectively; t_s and t_e are the start and end time of lane-changing, respectively. In order to solve the longitudinal trajectory, the Hamiltonian function in Eq. (2) is developed:

$$H_s = \frac{1}{2}j_s^2 + \lambda_{s1}\dot{s} + \lambda_{s2}\ddot{s} + \lambda_{s3}j_s \tag{2}$$

where λ_{s1}, λ_{s2}, and λ_{s3} are the Lagrangian operators corresponding to $\dot{s}$, $\ddot{s}$, and j_s, respectively. According to the Pontryagin's minimum principle (PMP) (Kim et al., 2011), the Hamiltonian function satisfies the in Eqs. (3)–(6) constraints:

$$\dot{\lambda}_{s1} = -\frac{\partial H_s}{\partial s} = 0 \Rightarrow \lambda_{s1} = c_{s1} \tag{3}$$

$$\dot{\lambda}_{s2} = -\frac{\partial H_s}{\partial v_s} = -\lambda_{s1} \Rightarrow \lambda_{s2} = -c_{s1}t + c_{s2} \tag{4}$$

$$\dot{\lambda}_{s3} = -\frac{\partial H_s}{\partial a_s} = -\lambda_{s2} \Rightarrow \lambda_{s3} = \frac{1}{2}c_{s1}t^2 - c_{s2}t + c_{s3} \tag{5}$$

$$0 = \frac{\partial H_s}{\partial j_s} = j_s + \lambda_{s3} \Rightarrow j_s = -\lambda_{s3} = -\frac{1}{2}c_{s1}t^2 + c_{s2}t - c_{s3} \tag{6}$$

According to the longitudinal jerk, the longitudinal acceleration, longitudinal velocity, and longitudinal displacement could be derived by

$$\ddot{s}(t) = -\frac{1}{6}c_{s1}t^3 + \frac{1}{2}c_{s2}t^2 - c_{s3}t + c_{s4} \tag{7}$$

$$\dot{s}(t) = -\frac{1}{24}c_{s1}t^4 + \frac{1}{6}c_{s2}t^3 - \frac{1}{2}c_{s3}t^2 + c_{s4}t + c_{s5} \tag{8}$$

$$s(t) = -\frac{1}{120}c_{s1}t^5 + \frac{1}{24}c_{s2}t^4 - \frac{1}{6}c_{s3}t^3 + \frac{1}{2}c_{s4}t^2 + c_{s5}t + c_{s6} \tag{9}$$

where c_{si} is the longitudinal quintic polynomial coefficient. Assuming that the initial longitudinal displacement, longitudinal velocity, and longitudinal acceleration are known, the longitudinal quintic polynomial coefficients can be obtained:

$$c_{s1} = 60[6t_e(v_{se} + v_{ss}) - 12s_e - (a_{se} - a_{ss})t_e^2]/t_e^5 \tag{10}$$

$$c_{s2} = 12[(14v_{se} + 16v_{ss})t_e - 30s_e - (2a_{se} - 3a_{ss})t_e^2]/t_e^4 \tag{11}$$

$$c_{s3} = 3[(8v_{se} + 12v_{ss})t_e - 20s_e - (a_{se} - 3a_{ss})t_e^2]/t_e^3 \tag{12}$$

$$c_{s4} = a_{ss} \tag{13}$$

$$c_{s5} = v_{ss} \tag{14}$$

$$c_{s6} = 0 \tag{15}$$

In order to minimize the fluctuation in longitudinal acceleration as much as possible, the vehicle velocity at the beginning and end of lane-changing is generally unchanged, there are $c_{s1} = 720(t_e v_s - s_e)/t_e^5$, $c_{s2} = 360(v_s t_e - s_e)/t_e^4$, $c_{s3} = 60(v_s t_e - s_e)/t_e^3$, $c_{s4} = 0$, $c_{s5} = v_s$, $c_{s6} = 0$. In addition, in order to keep the longitudinal fluctuation as lower as possible, it is necessary to reduce the longitudinal fluctuation, set $s_e = t_e v_s$. In this case, the longitudinal trajectory is

$$s(t) = v_s t \tag{16}$$

It could be seen from Eq. (16) that the longitudinal trajectory is mainly determined by the longitudinal velocity and lane-changing time.

2.2 Lateral derivation in FCS

Referring to the longitudinal trajectory planning process, the lateral trajectory planning results could be obtained:

$$l(t) = 6d_e t^5/t_e^5 - 15d_e t^4/t_e^5 + 10d_e t^3/t_e^5 \tag{17}$$

where d_e is the lateral displacement at the end of lane-changing, the standard lane-changing lateral distance of 3.75 m according to the common standards of Chinese roads. Equation (17) shows that the lane-changing time and lateral displacement mainly determine the lateral trajectory.

A two-dimensional trajectory could be synthesized after obtaining the longitudinal and lateral trajectory. From Eqs. (16) and (17), the lateral displacement of the lane-changing trajectory is generally fixed, and the vehicle velocity is also fixed when minimizing the longitudinal jerk. So only the lane-changing time is left as the only lane-changing trajectory parameter.

3 Data acquisition and analysis of natural lane-changing data for trajectory planning

The information about human drivers should be added after the basic lane-changing trajectory algorithm has been completed. To calculate the lane-changing trajectory more like the driving habits of human drivers from the planning level, the driving habits of human drivers should be collected. This paper uses an extended driving simulator to develop a scenario straight lane for a free lane-changing test in order to collect the lane-changing features of human drivers for trajectory planning. Compared to driving in real traffic, the extended driving simulator test does not fully simulate the driving experience, but still reflects the driving features of different drivers. In addition, the extended driving simulator test is more cost-effective and has a shorter development cycle without violating the test principles and design theory. The objective of this paper is to verify the feasibility of the principle of

the technical route. Many technical routes in the engineering field need to be tuned to practical applications. The results of the extended driving simulator test are therefore considered to be credible.

Lane-changing maneuvers are divided into free lane-changing and forced lane-changing. Forced lane-changing often occurs in scenarios where the vehicle has to change lanes due to traffic conditions, such as overtaking when the vehicle in front has a slow velocity, and the target lane has a small manoeuvrable area, or turning to avoid an obstacle that suddenly appears in the lane. The process of free lane-changing mostly occurs in urban scenarios with small traffic flow to ensure lane requirements, or in urban viaducts and highways with long vehicle spacing. The main difference between the two lies in the operable time of lane-changing and the operable road section. Free lane change could cover most lane-changing scenarios.

In practice, intelligent vehicles equipped with high-precision positioning equipment are collected, recorded, and processed to obtain a data set of driving features of lane-changing trajectory at different mean velocity bands. The data set is continuously updated through rolling calculations with a fixed-length window. Other data acquisition and analysis steps are identical to this section.

3.1 Experiment setup

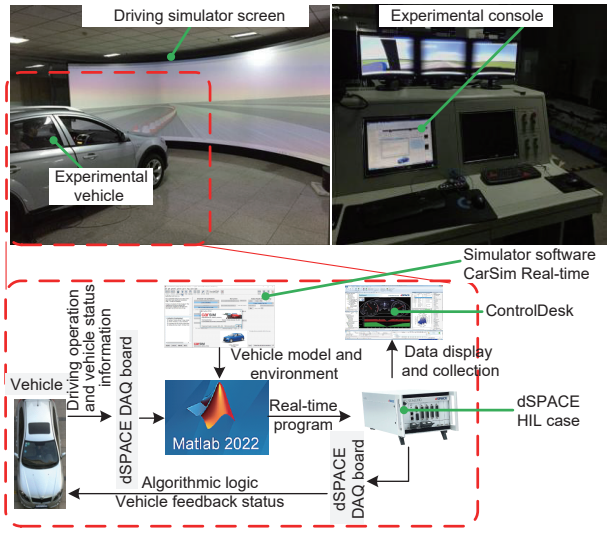

Fig. 2 Extended driving simulator.

The extended driving simulator used in this paper is shown in Fig. 2. The extended driving simulator adopts the dSPACE 1106 series controller and Simulink/CarSim real-time simulation platform. A 2 km long dual straight lane and random traffic vehicles were set in CarSim software, and 20 human drivers were recruited to change lanes freely at a constant velocity (V_x) of [10 m·s^{-1}, 30 m·s^{-1}] with 5 m/s intervals. The mean age of 20 human drivers was 24, and their driving years ranged from 1 to 7.

3.2 Lane-changing data analysis

In the 2 km long double straight lane, human drivers were asked many times to intercept the left and right lanes. In this paper, the collected 20 drivers' data were used for lane-changing trajectory interception and lane-changing feature analysis, respectively. The human drivers A and B's data were randomly selected for presentation, analysis, and design due to the limitation of article length. The lane-changing trajectories of human drivers A and B in five-velocity clusters are shown in Fig. 3. Then the features of lane-changing data were analyzed: the mean lane-changing time, the maximum slope of lane-changing trajectory, etc. The main lane-changing features of human drivers A and B in five-velocity clusters are shown in Fig. 4.

In Fig. 3, the lane-changing trajectories of human drivers A and B form respective trajectory clusters. In addition, with the increase in vehicle velocity, the lane-changing longitudinal distance increases. Fig. 4 shows that: (1) with the increase in vehicle velocity, the mean lane-changing times, and the maximum slopes of lane-changing trajectories of human drivers A and B show a decreasing trend; (2) at the same velocity, the lane-changing times, and the maximum slopes of lane-changing trajectories of human drivers A and B show a fluctuating pattern with a certain value as the center, respectively.

According to the law shown in Fig. 4, the multiple lane-changing of a human driver at a given velocity is regarded as a normally distributed process. Then the distribution of lane-changing times satisfies $Z_{tu} \sim N(\mu_{tu}, \sigma_{tu}^2)$. Where μ_{tu} is the mean lane-changing time for vehicle velocity u and σ_{tu} is the variance of the lane-changing times at vehicle velocity u. The mean value and variance of the lane-changing time and the maximum slopes of lane-changing trajectories at different velocities could be obtained in Table 1.

The features of human drivers A and B at different velocities are different: human driver B takes longer to change lanes than A, and the maximum slopes of changing lanes are smaller. It shows that human driver B is more cautious than A.

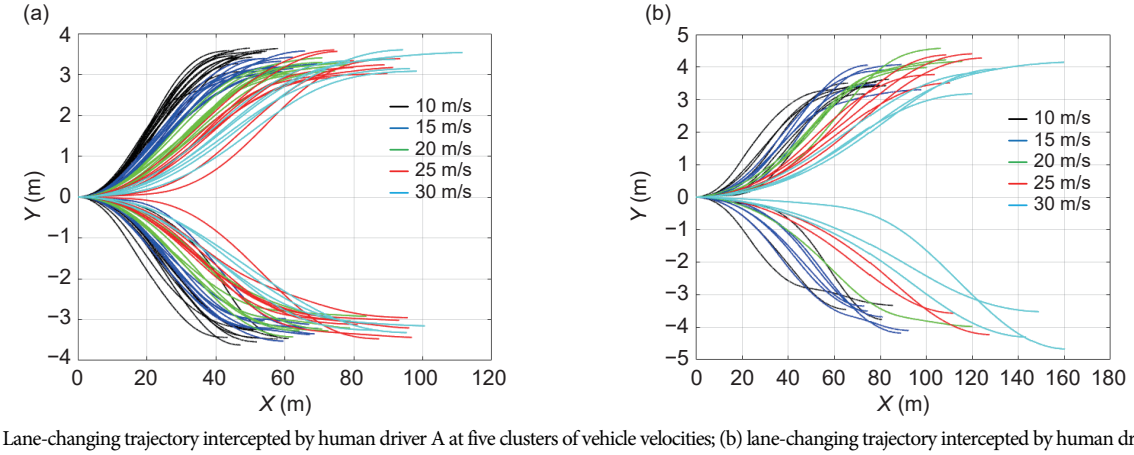

Fig. 3 (a) Lane-changing trajectory intercepted by human driver A at five clusters of vehicle velocities; (b) lane-changing trajectory intercepted by human driver B at five clusters of vehicle velocities.

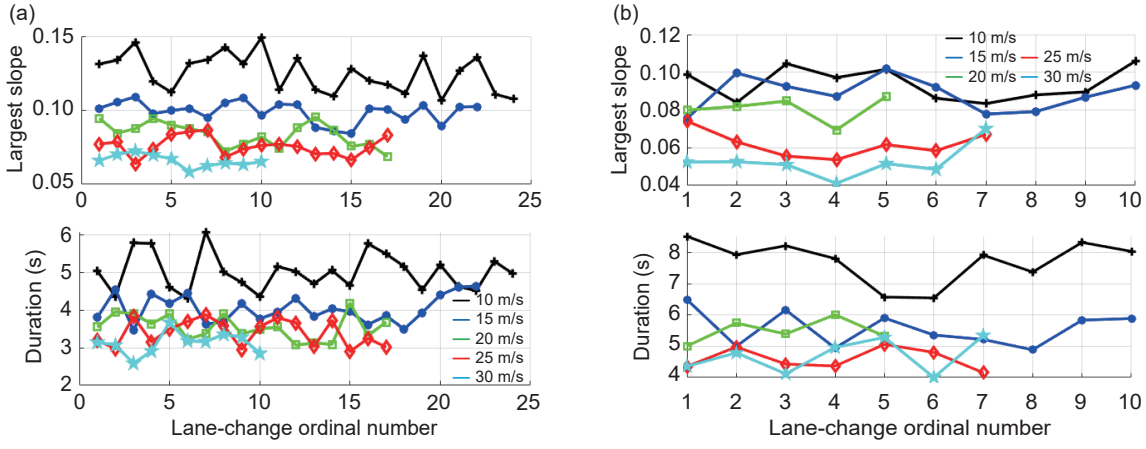

Fig. 4 (a) Main lane-changing features of human driver A at five vehicle velocities; (b) main lane-changing features of human driver B at five vehicle velocities.

Table 1 Lane-changing features of human drivers A and B

Driver	Feature	10 m·s^{-1}	15 m·s^{-1}	20 m·s^{-1}	25 m·s^{-1}	30 m·s^{-1}
A	Mean time	5.4 s	4.3 s	3.4 s	3.1 s	3.0 s
	Variance	0.6 s^2	0.4 s^2	0.3 s^2	0.2 s^2	0.2 s^2
	Mean maximum slope	0.1212	0.0957	0.0864	0.0722	0.0691
B	Mean time	7.72 s	5.57 s	5.49 s	4.59 s	4.69 s
	Variance	0.59 s^2	0.56 s^2	0.39 s^2	0.35 s^2	0.54 s^2
	Mean maximum slope	0.0939	0.0886	0.0807	0.0619	0.0525

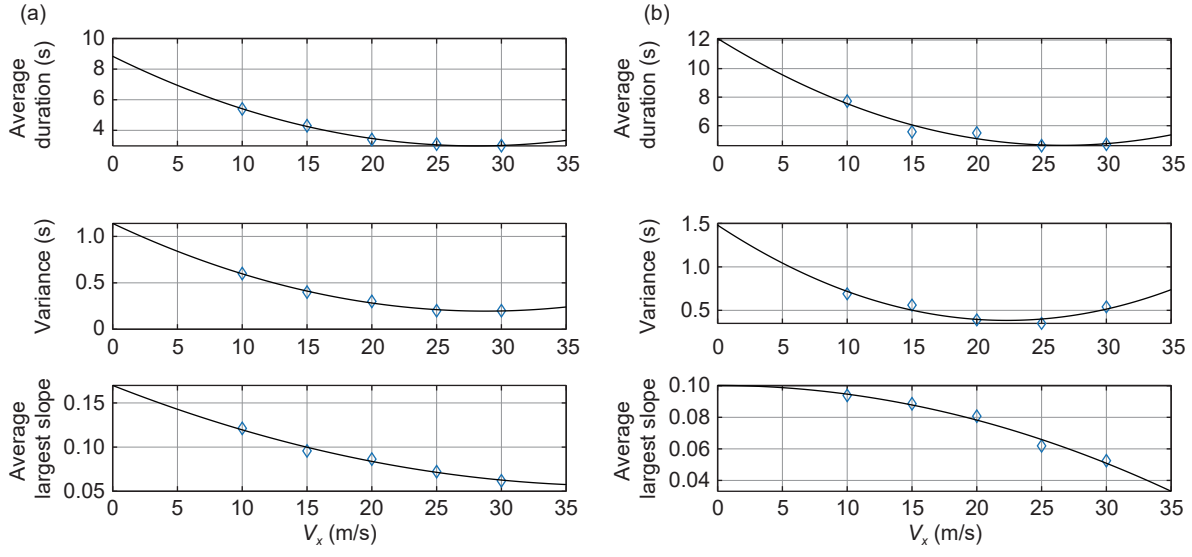

Fig. 5 (a) Main feature values of human driver A corresponding to the whole velocity range; (b) main feature values of human driver B corresponding to the whole velocity range.

According to the above features, the vehicle velocity is used as the abscissa to fit, and then the features in the whole velocity range are deduced. The fitting features corresponding to the whole velocity range are shown in Fig. 5.

4 Highly human-like lane-changing trajectory planning based on human driver features

In this section, the basic trajectory clusters based on the collected information of human drivers and the mean lane-changing time are generated and perform constrained optimization solving. The highly human-like lane-changing trajectory could be obtained through trajectory synthesis and coordinate system transformation, trajectory stability search, optimal trajectory search, and collision avoidance detection.

4.1 Trajectory synthesis and coordinate system transformation

Based on the minimization fluctuation-based lane-changing trajectory expression derived in Section 2 and the analysis of the influencing factors, the expression of the lane-changing trajectory at a fixed velocity is simplified to a function with the lane-changing time as the only independent variable. The theoretical idea of human-like lane-changing trajectory is proposed in this paper: based on the collected lane-changing time features of drivers, a fixed spacing search is conducted to generate a set of trajectory clusters, and then the final human-like lane-changing trajectory is obtained by using objective function optimization.

In this paper, based on the collected lane-changing data of a particular driver, we generated trajectory clusters at fixed intervals

based on the mean lane-changing time of that human driver as the center and a range of positive and negative 5 times the lane-changing time as the range. That is, the range of lane change times for the trajectory clusters is $[\mu_{tu} - 5\sigma_{tu}, \mu_{tu} + 5\sigma_{tu}]$. Although the normal distribution already has a 99% probability sum for a range of positive and negative 2.58 times the standard deviation, the range of positive and negative 5 times the standard deviation is still chosen in this paper considering planning completeness. In the absence of special circumstances, the lane-changing features of a given single human driver at a given velocity are stable. Even if extreme conditions occur in practice, the influence of outliers on the collected information would be reduced due to the continuously updated historical lane-changing data. Therefore, the trajectory cluster is nearly stable. In a specific scenario, the coordinate system is converted to GCS. The lane-changing features of selected human drivers A and B at five sets of vehicle velocities are shown in Fig. 4.

The main factors affecting the number of trajectories generated and the calculation time in this session are the variances of historical lane-changing time and the fixed spacing step size. When the variance of historical lane-changing time is large, more trajectories are generated. When the spacing step size is smaller, more trajectories are generated. However, a larger number of trajectories means that the trajectories are closer to being complete.

In this section, to balance the contradiction between calculation time and completeness, clusters of trajectories in the FCS are generated for natural drivers A and B at vehicle velocities of 10 and 15 m·s^{-1}, respectively, with lane-changing interval of 0.2 s (Fig. 6). A circular road in CarSim software is selected as the planning scenario and intercepted the center line of a section of road for coordinate system transformation, as shown in Fig. 7. The route includes curves and straight lines of varying curvature, which is a typical suburban route. Two planning scenarios are selected. The first part is the curve with moderate curvature, which corresponds to the lane-changing operation on the road with curvature in a real scenario. The second part is the straight lane, which corresponds to the free lane-changing or forced lane-changing on the expressway or motorway in the real scenario. The planning scenario and conversion trajectory clusters are shown in Fig. 7.

Fig. 7(b) is converted from Fig. 6(a) and contains 30 trajectories. Fig. 7(c) is converted from Fig. 6(b) and includes 21 trajectories. Fig. 7(d) is converted from Fig. 6(c) and includes 36 trajectories. Fig. 7(b) is converted from Fig. 6(a) and includes 26 trajectories. The generated trajectories would be used for search optimization in later sections.

4.2 Trajectory stability search

Due to the varying distribution of lane-changing time and differing actual road center lines of human drivers, the generated trajectory clusters may contain trajectories not conforming to vehicle stability requirements. This situation is typically found in local planning algorithms where vehicle kinematic properties are not taken into account. Therefore, the number of current search rounds is increased to remove unstable trajectories and retain only clusters that meet the stability requirements. On the one hand, the reference road center lines have different curvatures, leading to

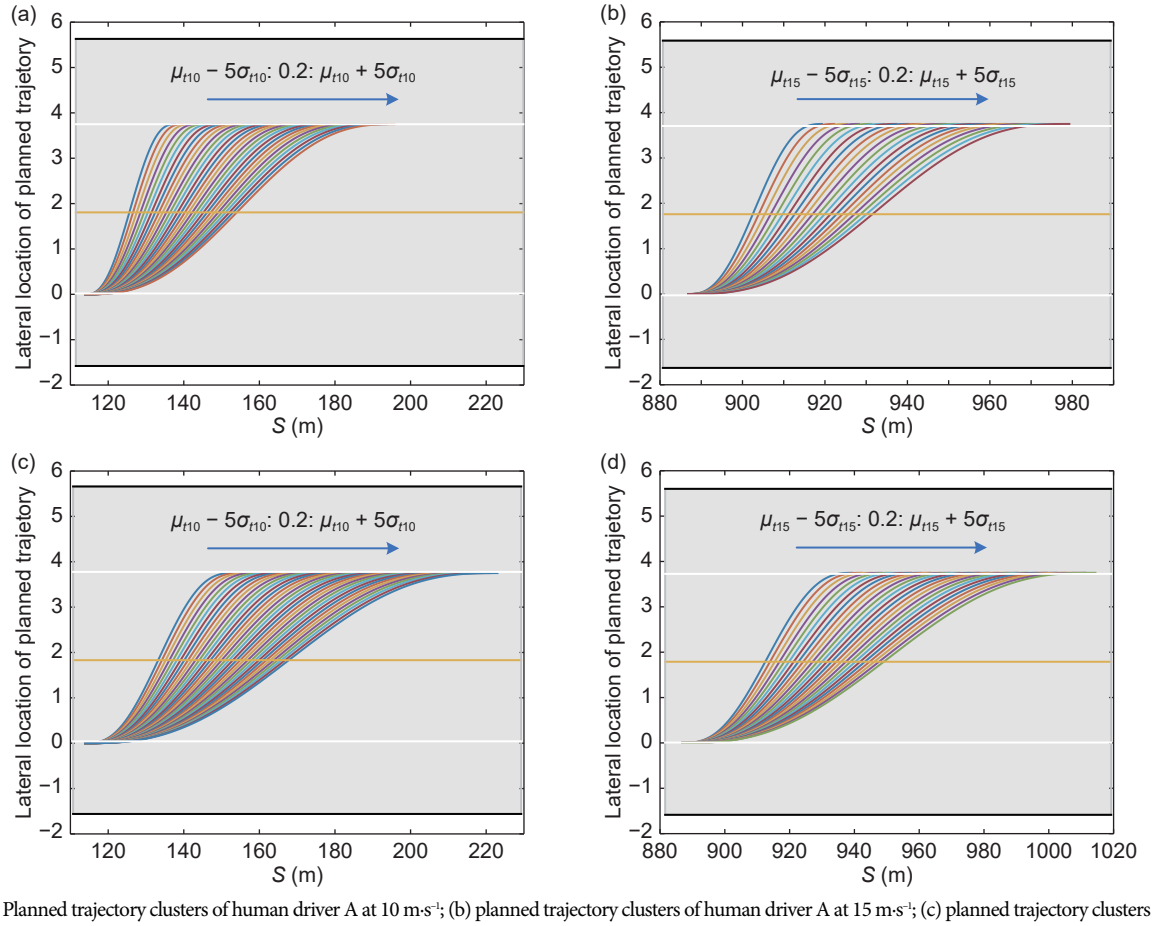

Fig. 6 (a) Planned trajectory clusters of human driver A at 10 m·s^{-1}; (b) planned trajectory clusters of human driver A at 15 m·s^{-1}; (c) planned trajectory clusters of human driver B at 10 m·s^{-1}; (d) planned trajectory clusters of human driver B at 15 m·s^{-1}. Different colors in the trajectory cluster represent different trajectories.

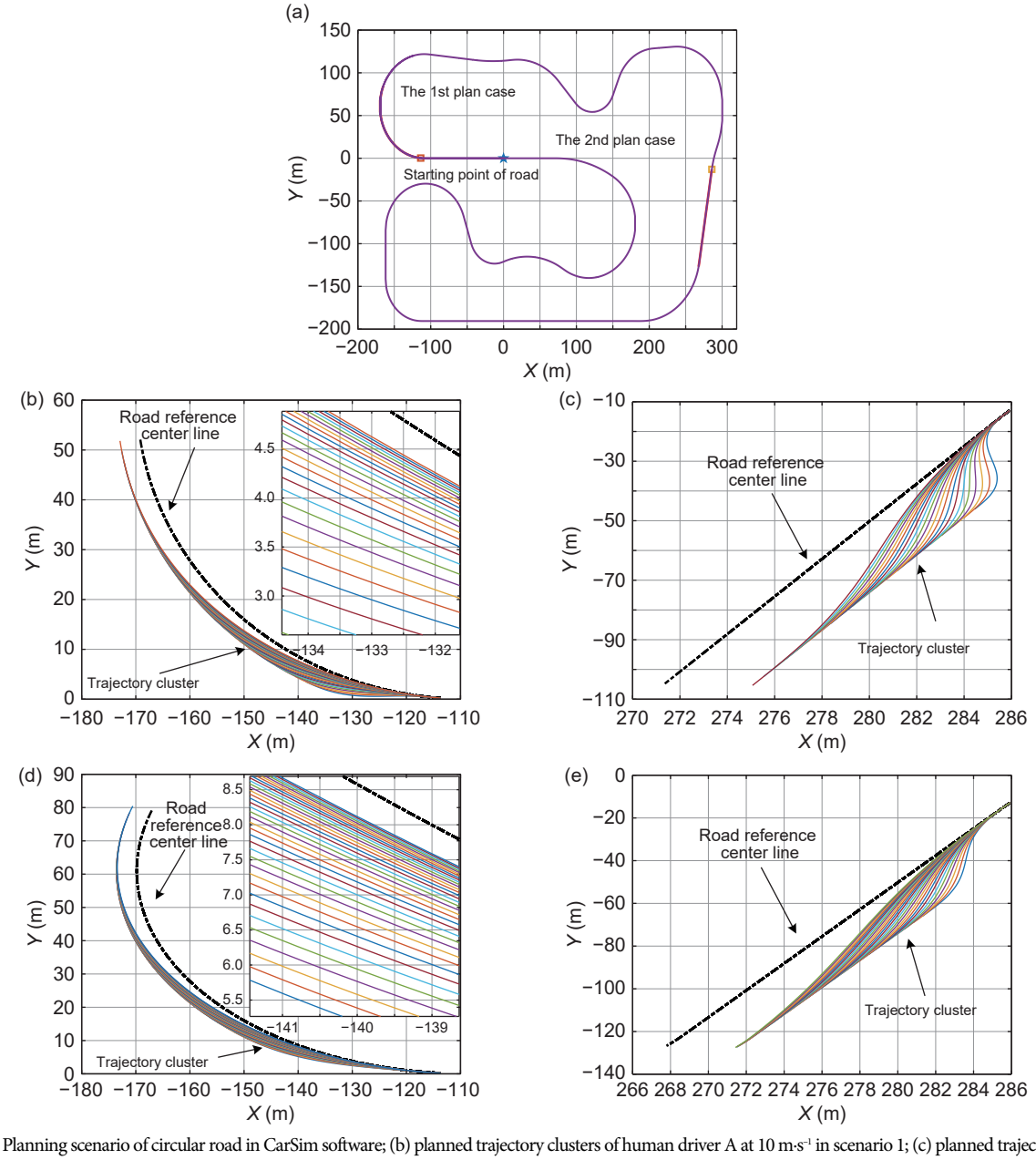

Fig. 7 (a) Planning scenario of circular road in CarSim software; (b) planned trajectory clusters of human driver A at 10 m·s^{-1} in scenario 1; (c) planned trajectory clusters of human driver A at 15 m·s^{-1} in scenario 2; (d) planned trajectory clusters of human driver B at 10 m·s^{-1} in scenario 1; (e) planned trajectory clusters of human driver B at 15 m·s^{-1} in scenario 2. Different colors in the trajectory cluster represent different trajectories.

extensively obtaining the vehicle dynamics states at different vehicle velocities and trajectories with a large and difficult workload. On the other hand, the maximum lateral acceleration limit method is selected to improve the operational efficiency and to expand the application range of the stability search algorithms. With the lateral acceleration of 0.4 g as the limiting instability condition, only the trajectory with the maximum lateral acceleration of less than 0.4 g (Zhao et al., 2019) could satisfy the requirement of trajectory stability.

For the GCS trajectories, the first-order and second-order derivatives of the plan in the X and Y directions are fitted with S as the baseline, respectively. Then, the curvatures of the trajectories and the lateral acceleration of the trajectories are calculated according to Eqs. (18) and (19):

$$\rho = (x'y'' - y'x'')/[(x')^2 + (y')^2] \tag{18}$$

$$\hat{a}_y = v_x^2\rho \tag{19}$$

where ρ is the curvature; $\hat{a}_y$ is the theoretical lateral acceleration of the planned trajectory. $x' = \mathrm{d}x/\mathrm{d}s$; $x'' = \mathrm{d}^2x/\mathrm{d}s^2$; $y' = \mathrm{d}y/\mathrm{d}s$; $y'' = \mathrm{d}^2y/\mathrm{d}s^2$.

The lateral accelerations corresponding to the trajectory clusters of human drivers A and B in the scenarios are shown in Fig. 8. The trajectories with the maximum lateral acceleration greater than 0.4 g are deleted, and the stable trajectory clusters after searching are shown in Fig. 9.

In Fig. 8, in the two scenarios of human driver A, the planned trajectory clusters contain trajectories whose maximum lateral accelerations are more than 0.4 g. Under scenario 1, three trajectories exceed the 0.4 g stability threshold. Under scenario 2, one trajectory exceeds the 0.4 g stability threshold. Moreover, the trajectories that exceed the stability threshold all start in the direction of the shortest lane-changing time. In contrast, all

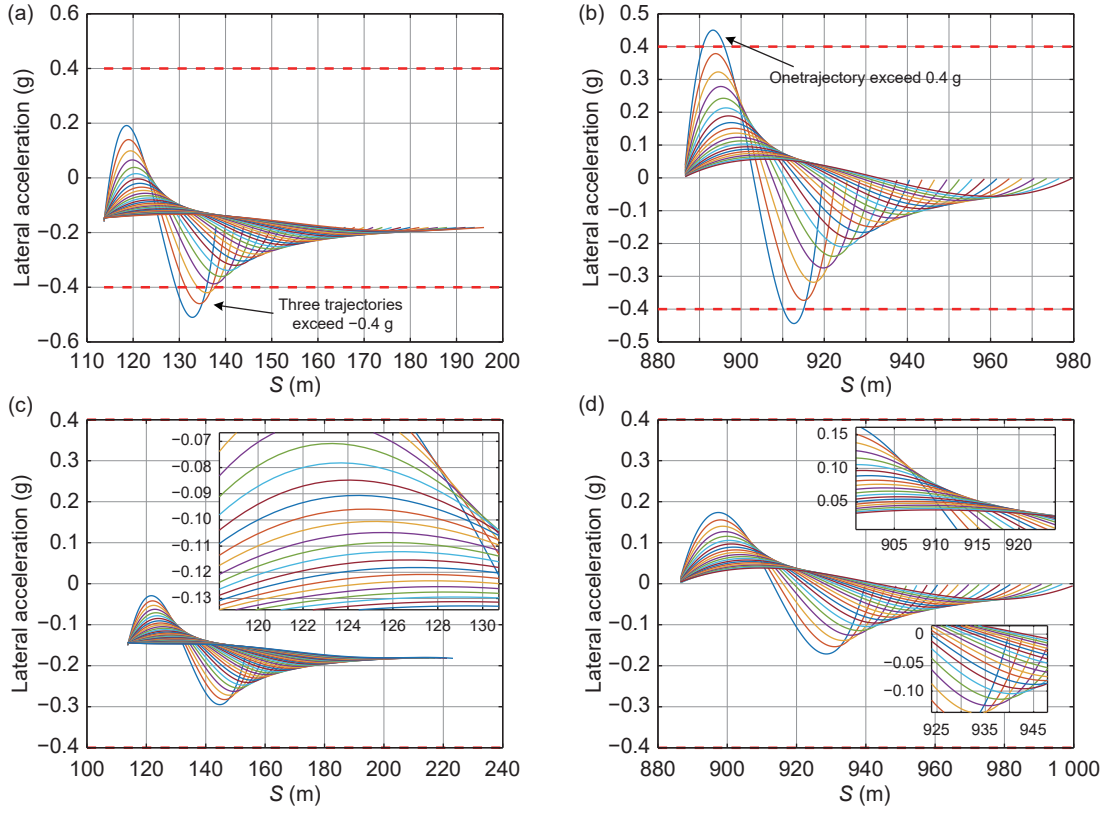

Fig. 8 (a) Planning scenario of circular road in CarSim software; (b) planned trajectory clusters of human driver A at 10 m·s^{-1} in scenario 1; (c) planned trajectory clusters of human driver A at 15 m·s^{-1} in scenario 2; (d) planned trajectory clusters of human driver B at 10 m·s^{-1} in scenario 1; (e) planned trajectory clusters of human driver B at 15 m·s^{-1} in scenario 2.

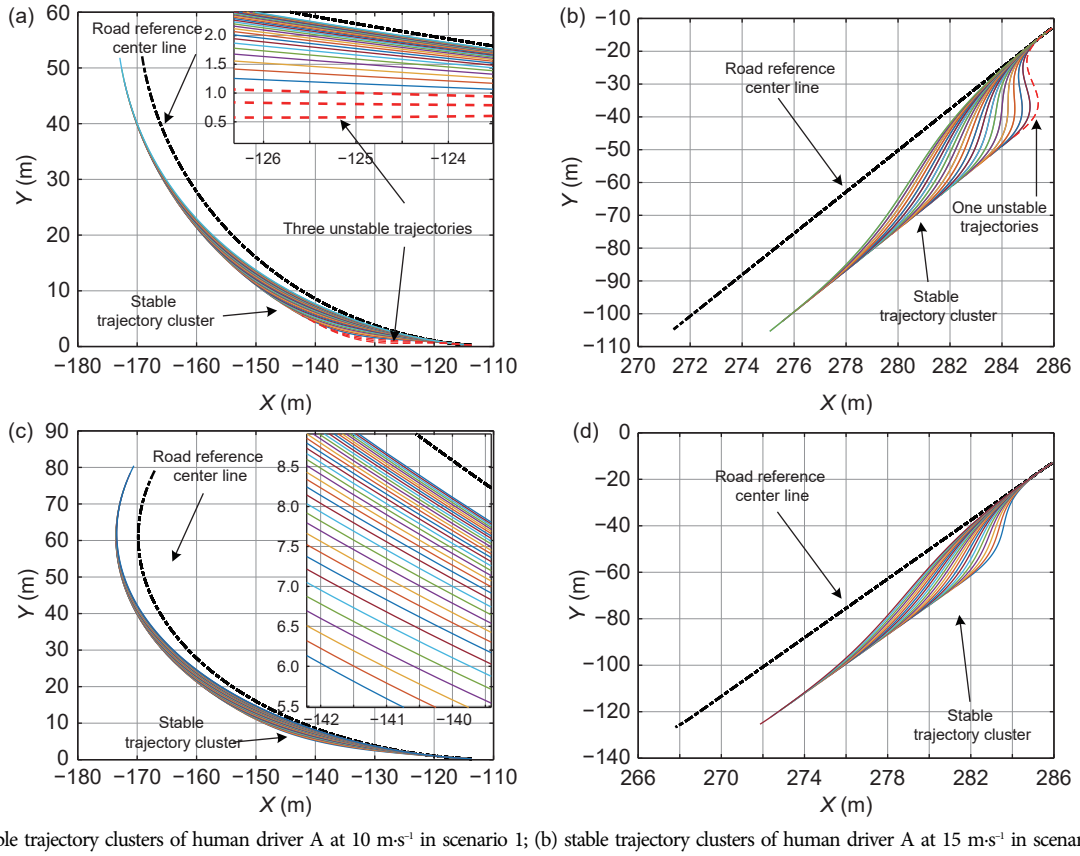

Fig. 9 (a) Stable trajectory clusters of human driver A at 10 m·s^{-1} in scenario 1; (b) stable trajectory clusters of human driver A at 15 m·s^{-1} in scenario 2; (c) stable trajectory clusters of human driver B at 10 m·s^{-1} in scenario 1; (d) stable trajectory clusters of human driver B at 15 m·s^{-1} in scenario 2. The stable trajectories are depicted by the solid line, and the rejected unstable trajectories are depicted by the dashed line.

https://doi.org/10.26599/JICV.2023.9210004

trajectories of human driver B satisfy the stability requirements in both scenarios. The reason is that human drivers have different driving features and different needs for trajectories. It also proves the necessity for FCS planning and the independent case of each human driver. Compared with Fig. 7, the unstable trajectories have been eliminated in Fig. 9.

4.3 Optimal trajectory search and collision avoidance detection

For searching out the final execution trajectory, the cost function of each trajectory is developed after the stability search, and the trajectory with the minimum cost is selected for collision avoidance detection. The trajectory passing collision avoidance detection is the final optimal planned trajectory.

4.3.1 Optimal trajectory search

In the process of trajectory planning optimization based on quintic polynomial, the cost function can be developed according to the design requirements, and the trajectory with the minimum search cost can be used as the optimal trajectory. To develop a lane-changing trajectory close to the features of human drivers, this paper focuses on the following three cost indicators: personalization indicator, smoothness indicator, and lane-changing efficiency indicator.

As the core indicator of human-like trajectory planning, the rationality of its establishment would greatly determine the goodness of trajectories. According to the analysis of the lane-changing trajectory of human drivers, the features of human drivers' lane-changing are mainly reflected in the mean lane-changing time and the maximum slopes of lane-changing trajectories. In other words, if the mean lane-changing time and maximum slope of the planned trajectory could be closer to that of the driver's historical lane-changing trajectory cluster, it represents that the planned trajectory can better match natural drivers' lane-changing driving habits. Since the data of human drivers' lane-changing are collected on the straight road, the final trajectory is affected by the actual road center line, the maximum slope term should be compared in FCS. The human-like cost is set to two items, namely, the proximity term of the lane-changing times and the proximity term of the maximum slope of trajectories, and the expression is

$$c_{p\_te}^{j} = (t_{\mathrm{e}}^{j} - t_{\mathrm{dr}})^2 / t_{\mathrm{dr}} \tag{20}$$

$$c_{p\_s}^{j} = (k_{\mathrm{m}}^{j} - k_{\mathrm{am}})^2 / k_{\mathrm{am}} \tag{21}$$

where $c_{p\_te}^{j}$ is the proximity cost of lane-changing time of the j-th trajectory; t_e^j is the lane-changing time of the j-th trajectory; t_{dr} is the mean lane-changing time of human drivers at the current velocity; $c_{p\_s}^{j}$ is the proximity cost of the maximum slope of the j-th trajectory; k_{m}^{j} is the maximum slope of the j-th trajectory; k_{am} is the mean maximum slope of human drivers at the current velocity.

As an important indicator of trajectory planning, the smoothness indicator affects the ride comfort. The trajectory developed in this paper is based on the minimum longitudinal fluctuation, so the longitudinal fluctuation cost could not be considered when developing the cost function. People in the vehicle are more sensitive to lateral fluctuation, so the lateral stability design should be considered. In this paper, the lateral acceleration is designed as the lateral stability feature, and the objective is to minimize the lateral acceleration of the planning trajectory. The smoothness indicator expression is as Eq. (22):

$$c_{\mathrm{s}}^{j} = \left[\sum_{i=1}^{n} (\hat{a}_{yi}^{j}/4)^2\right] / n \tag{22}$$

where c_{s}^{j} is the lateral stability cost of the j-th trajectory; $\hat{a}_{yi}^{j}$ is the lateral acceleration at the i-th point of the j-th trajectory; n is the planning point value.

The lane-changing efficiency refers to the time from the beginning to the end of the lane change. Therefore, the shorter the lane-changing time, the higher the lane-changing efficiency. In this paper, the expression of the lane-changing efficiency indicator is as Eq. (23):

$$c_{\mathrm{e}}^{j} = (t_{\mathrm{e}}^{j}/t_{\mathrm{e}}^{\mathrm{m}})^2 \tag{23}$$

where c_{e}^{j} is the lane-changing efficiency cost of the j-th trajectory, t_{e}^{m} is the maximum lane-changing time, and m is the sequence number of the longest lane-changing time trajectory.

According to the purpose of establishing lane-changing trajectory, the weights of the above four cost indicators are assigned. In order to reflect the human-like degree of the trajectory as much as possible, the subjective parameter method is chosen in this paper. It is worth noting that although the subjective parameter method could impose limitations to the application of the algorithm, it satisfies the problem-solving objective of this paper. Moreover, the results of the subjective parameter method are more satisfied with expectations. The weight of lane-changing time, w_{p_te}, is set to 0.3, and the weight of the maximum slope approach term, w_{p_s}, is set to 0.2. The weight of smoothness cost, w_{s}, is 0.3, and the weight of lane-changing efficiency cost, w_{e}, is 0.2. It is necessary to emphasize that the parameter settings depend on the importance that the designer places on the different indicators.

The final cost function is as Eq. (24):

$$c^{j} = [w_{p\_te} \quad w_{p\_s} \quad w_{\mathrm{s}} \quad w_{\mathrm{e}}][c_{p\_te}^{j} \quad c_{p\_s}^{j} \quad c_{\mathrm{s}}^{j} \quad c_{\mathrm{e}}^{j}]^{\mathrm{T}} \tag{24}$$

where c^j is the lane-changing cost of the j-th trajectory. According to Eq. (24), the cost value of each trajectory is obtained, and then the minimum cost value is searched as the optimal planned trajectory.

$$c^{j*} = c_{\min}^{j} = \min(c^{j}) \tag{25}$$

4.3.2 Optimal trajectory search

The cost function could not be developed simply as a particle because the vehicle occupies a certain volume of space. However, the collision cost term is not considered in the cost function. To guarantee the absolute safety of the planned trajectory, it is necessary to perform the collision avoidance detection on the optimal trajectory (Xue et al., 2019). If the collision avoidance detection is passed, the optimal trajectory is the final output of the optimal human-like planned trajectory. On the contrary, if collision avoidance detection fails, it is necessary to remove the optimal trajectory from the original stable trajectory clusters. After that, it will search for the optimal trajectory once again, and carry out the collision avoidance detection until the planned trajectory has completed the collision avoidance detection.

In this paper, vehicles and obstacles are simplified as convex rectangles on the ground plane. Most conventional collision detection methods for the feature points and their corresponding motion vectors are mostly transplanted from the two-dimensional

game area (Chae et al., 2017). The main methods include the center distance detection method, projection line method, and vector crossing method. However, some methods are not applicable to the collision detection of convex rectangles with angles, and others have complicated calculation processes, resulting in huge calculation volumes. This paper proposes a new collision detection algorithm, the vertex embedding method, which is used for convex polygons. The principle of this method is shown in Fig. 10. There are two rectangles, ABCD and EFGH. The four vertices of rectangular ABCD and rectangle EFGH are connected in pairs to form 16-line segments. Each vertex has four lines, which form four angles with the baseline. If a vertex of the rectangle ABCD is inside the rectangle EFGH, the four angles formed by the vertex would be in four quadrants. On the contrary, when the vertex is outside another rectangle, the four angles formed by the vertex are most in two quadrants.

Collision detection is divided into dynamic obstacle detection and static obstacle detection. In order to minimize the volume of calculation, the distance between the planned trajectory and the dynamic obstacle vehicle is determined first, and collision detection is carried out when the distance between them is less than a certain extent. This step of processing would reduce the operation time of the algorithm. For static obstacle detection, only the nearest trajectory point is detected. The convex fitting shape and size of static and dynamic obstacles are determined based on perceptual information. Table 2 shows the collision detection algorithm developed in this paper according to the principle of the vertex embedding method.

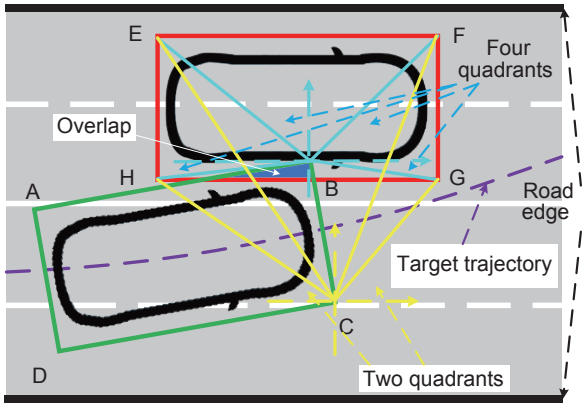

Fig. 10 Schematic diagram of vertex embedding method.

where $s\_p^*(t)$, $l\_p^*(t)$, $\theta\_p^*(t)$, and t_p^* are the longitudinal, lateral, route, and time points of the optimal trajectory in FCS, respectively; *s_dynamic_s*, *l_dynamic_s*, and v_x*_dynamic* are the longitudinal starting point, lateral starting point, and longitudinal velocity of the dynamic obstacle in FCS, respectively; *s_static_s*, *l_static_s* are the longitudinal point and the lateral point of the static obstacle in FCS, respectively; *d_threshold* is the distance threshold between the obstacle and the vehicle; *l_v*, *w_v* are the length and width of the obstacle, respectively; *Trigger_collision* is

Table 2 Collision detection algorithm

Algorithm 1. The collision detection algorithm based on vertex embedding method

Input: $s\_p^*(t)$, $l\_p^*(t)$, $\theta\_p^*(t)$, t_p^*, *s_dynamic_s*, *l_dynamic_s*, v_x*_dynamic*, *s_static_s*, *l_static_s*, *d_threshold*, *l_v*, *w_v*

1. Predicting based on constant velocity:

$s\_dynamic(t) = v_x\_dynamic \times t\_p^*$; $l\_dynamic(t) = l\_dynamic\_s$;

2. The deletion of dynamic obstacle distance and static obstacle distance:

If $(s\_p^*(t) - s\_dynamic(t))^2 + (l\_p^*(t) - l\_dynamic(t))^2 < d\_threshold^2$

Output $t\_d = t$

End

If $\min((s\_p^*(t) - s\_static\_s)^2 + (l\_p^*(t) - l\_static\_s)^2)$ is true

Output $t\_s = t$

End

3. Calculating the vertices of vehicles and obstacles

4. Calculating the angle of the vertex line:

For i = 1:8

$\theta_i(t\_d)$ = function_calculating_angle($vertex\_line\_y_i(t\_d)$, $vertex\_line\_x_i(t\_d)$);

$\theta_i(t\_d)$ = function_calculating_angle($vertex\_line\_y_i(t\_s)$, $vertex\_line\_x_i(t\_s)$);

End

5. Calculating the difference between the maximum and minimum of the four angles of the vertex:

For i = 1:8

$\theta_{max\_min\_i}(t\_d) = \max(\theta_i(t\_d)) - \min(\theta_i(t\_d))$;

$\theta_{max\_min\_i}(t\_s) = \max(\theta_i(t\_s)) - \min(\theta_i(t\_s))$;

End

6. Judging the collision result:

If $\theta_{max\_min\_i}(t\_d) < \pi$ && $\theta_{max\_min\_i}(t\_s) < \pi$

Trigger_collision = 1;

Else

Trigger_collision = 0;

End

Output: *Trigger_collision*

the result of collision detection algorithm, which equals to 1 means that the track does not collide, and equals to 0 means that the trajectory would collide.

If *Trigger_collision* is 1, the optimal trajectory is the final planned trajectory. Conversely, if *Trigger_collision* is 0, the optimal trajectory is deleted from the trajectory clusters. After that, the optimal trajectory search and collision avoidance detection are performed again until the planned trajectory is output through collision avoidance detection, and the cycle ends.

Finally, the planned lane-changing trajectory must satisfy the vehicle stability and collision safety constraints.

4.3.3 Summary of planning algorithm

When the safe trajectory clusters do not satisfy the collision avoidance detection, no lane-changing trajectory would be generated. At this point, the planning layer conflicts with the decision layer and requires the decision layer to re-execute the confirmation. As the logic algorithm of the decision layer is not covered in this paper, it would not be discussed. When the lane change trajectory is not generated, the vehicle would continue to travel along the original lane.

In terms of the trajectory planning process in this paper, the optimization objective is firstly proposed to generate the basic trajectory clusters. Subsequently, the trajectory clusters are subjected to an optimization search and a constraint search. In this paper, the optimization constraint process proposed is decentralized. This process of optimal trajectory planning is the same as the one proposed by Zhou et al. (2019). However, it is different from the nonlinear programming (NLP) problems with uniform optimization constraints proposed by Li et al. (2020). The discrete steps do not pose an NLP problem and make it easier to know the specifics of the planning process.

According to the human-like means, the trajectory planning optimization method and optimization process that this paper focuses on is summarized in Table 3 to compare the difference between the lane-changing trajectory planning algorithms proposed. It is worth noting that the optimization method mentioned in Table 3 refers to the optimization method adopted for trajectory planning rather than improving a certain step.

Table 3 shows that this paper is significantly different from relevant studies in the comprehensive treatment of human-like means, optimization methods, and optimization processes. In terms of human-like means, the statistical method is used to avoid unexpected extremes, while keeping the algorithm process simple, the results credible, completeness, and interpretable. In terms of optimization methods and processes, the distributed optimization search first and the subsequent collision avoidance detection structure would lower the calculation difficulty in principle.

5 Verification of trajectory planning and tracking

In this section, the three objectives of the algorithm are verified through the planning procedure and tracking procedure: (1) to validate the execution of the algorithm, the planning results of the planning algorithm under different vehicle velocities and scenarios are solved; (2) to demonstrate the potential of the human-like planning trajectory in the field of trajectory prediction and to mitigate the potential conflict between human driver and automatic system, the fitting degree of the planning trajectory relative to the lane-changing trajectory of human driver is verified; (3) to verify the feasibility of the planned trajectory for the tracking layer of intelligent vehicle, a tracking simulation program is developed to track and verify the trajectory. The simulation procedure operated on a desktop computer with an Intel i5-7300HQ CPU (2.5 GHz), 16.0 GB RAM, Microsoft Windows 10 (64-bit), and MATLAB 2018a (64-bit).

5.1 Human-like trajectory planning with obstacles

In order to verify the feasibility of the algorithm, a dynamic obstacle vehicle is set up in the target lane with the starting position of (s_s, d_e) and the velocity of $0.4v_s$ while a static obstacle vehicle is set up in the starting lane with a position of (s_s + 57.68, 0), according to the process described above. The static and dynamic obstacle vehicles are fitted into a rectangle with a length of 2.9 m and a width of 2.5 m. In the above scenarios, the planned trajectory is obtained, as shown in Fig. 11.

Figs. 11(a), 11(c), 11(e), and 11(g) show the planned trajectory of human drivers A and B for scenarios 1 and 2 at 10 and 15 m·s^{-1} velocities, respectively. Figs. 11(b), 11(d), 11(f), and 11(h) place the planned trajectory under a cluster of experimentally collected trajectories. The results show that the planned trajectories vary between drivers at different vehicle velocities and scenarios, and the planned trajectories are the same as the collected trajectory clusters. It is not significantly beyond the actual track clusters.

The planned lane-changing time of human drivers A and B for scenarios 1 and 2 at 10 m·s^{-1} and 15 m·s^{-1} velocities are 5.0257, 3.9971, 6.5551, and 4.9434 s, respectively. The differences in the mean time of lane-changing collected from human drivers A and B are 0.3743, 0.3029, 1.1649, and 0.6266 s, with the relative difference of 6.9%, 7.04%, 15.09%, 11.25%, respectively,. The planned results show that: (1) the performance of the algorithm is high in terms of executability; (2) the human-like degree of planned trajectory is high, which belongs to the high-level

Table 3 Algorithm comparison

Ref.	Human-like means	Optimization method	optimization process
This paper	Based on the normal distribution features of historical lane changing trajectory clusters; Quintic polynomial	Distributed optimization search	Optimization search before collision avoidance detection
Zhang et al. (2019)	Single fitting based on a lane changing trajectory; Cubic polynomial	Coincidence degree with acquisition trajectory	No collision avoidance detection
Wang et al. (2016)	Single fitting based on a lane changing trajectory; Sine function	None	None
Zhu et al. (2018)	Factor analysis, fuzzy *c*-means clustering and back-propagation neural network for classification; Sine and cosine functions	None	None
Li et al. (2020)	None	Nonlinear programming with unified optimization constraints	The optimization process includes collision avoidance constraints
Zhou et al. (2019)	None	Distributed optimization search	Optimization search contains collision avoidance items

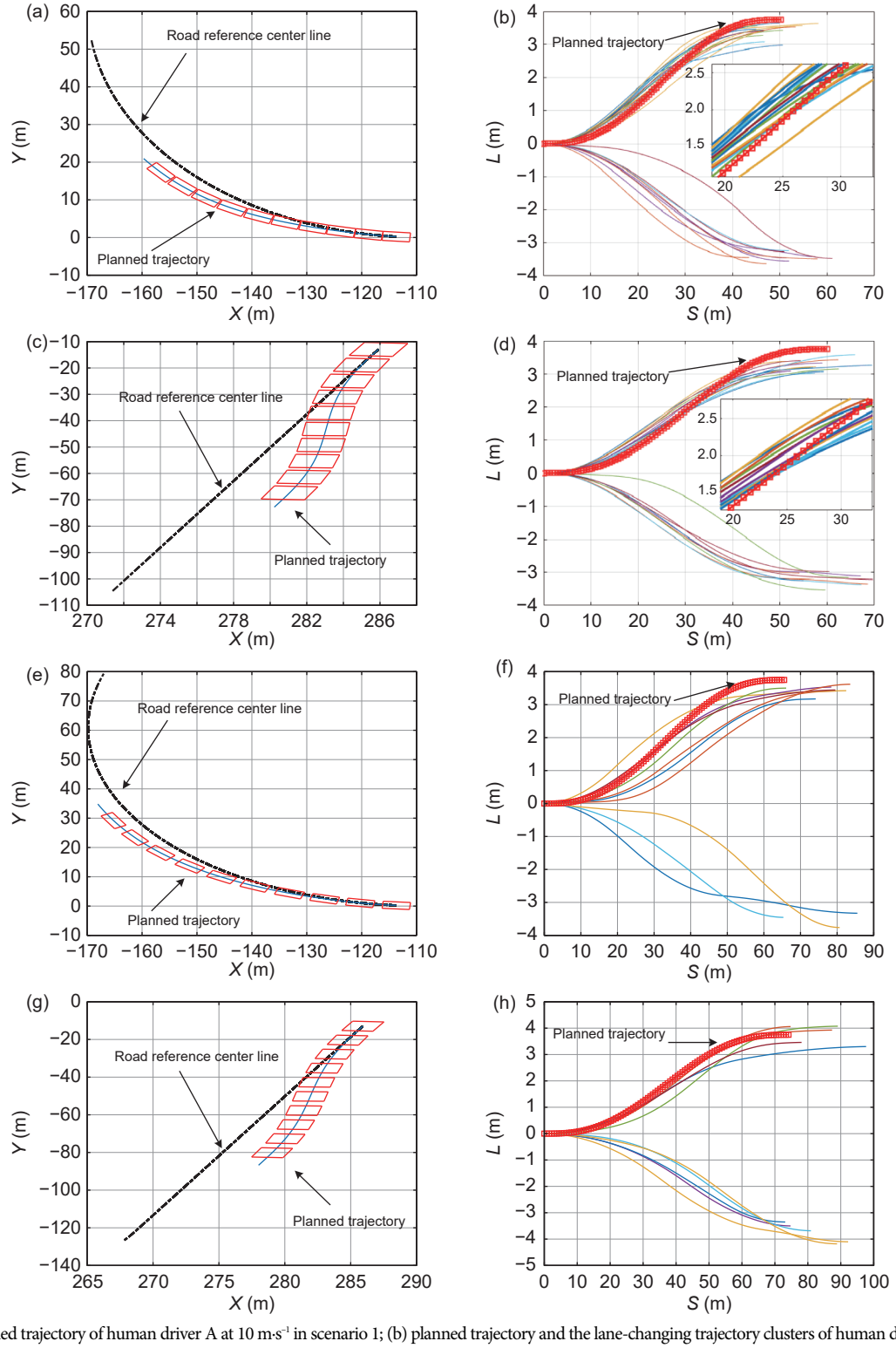

Fig. 11 (a) Planned trajectory of human driver A at 10 m·s^{-1} in scenario 1; (b) planned trajectory and the lane-changing trajectory clusters of human driver A at 10 m·s^{-1}; (c) planned trajectory of human driver A at 15 m·s^{-1} in scenario 2; (d) planned trajectory and the lane-changing trajectory clusters of human driver A at 15 m·s^{-1}; (e) planned trajectory of human driver B at 10 m·s^{-1} in scenario 1; (f) planned trajectory and the lane-changing trajectory clusters of human driver B at 10 m·s^{-1}; (g) planned trajectory of human driver B at 15 m·s^{-1} in scenario 2; (h) planned trajectory and the lane-changing trajectory clusters of human driver B at 15 m·s^{-1}.

personalization. (3) the planned human-like trajectory is the highly fitting degree for the human driver's trajectory change.

The total calculation time of the planners in the four cases was 0.321 s, 0.376 s, 0.381 s, and 0.379 s, respectively. Since the planning algorithm in this paper is improved and applied based on the reference (Zhou et al., 2019), this paper selects the calculation time in this reference as the comparison object. The calculation time of the three scenarios in Zhou et al. (2019) is 0.687, 0.772, and 0.828 s, respectively. The calculation time of this paper is 44%–61% faster than that of the reference (Zhou et al., 2019). The improvement in completion time is explained by the fact that the algorithm only calculates the collision avoidance detection for points within the closest range of the optimal trajectory from the obstacle, rather than searching for the optimal

trajectory from all the collision avoidance safety trajectories.

5.2 Function verification of trajectory prediction based on the historical information

The high fitting of human-like trajectory to the lane-changing trajectory of human drivers provides strong potential for practical applications: (1) it enables trajectory prediction based on historical information; (2) it allows for the mitigation of potential trajectory conflict between human driver and automatic system at the planning level. First, it is proposed that the planned human-like trajectory could reflect the lane-changing trajectory to a certain extent, i.e., lane-changing trajectory prediction. The human-like trajectory could be broadcast through V2V communication equipment in the intelligent traffic flow (Wu and Qu, 2022). Simultaneously, the trajectory is a potential lane-changing trajectory to be executed by the primary vehicle for the other vehicles that receive it. Secondly, when the planned lane-changing trajectory is close to the expected trajectory of the human driver, the human driver could further reduce the additional driving burden caused by the human-machine trajectory conflict, and the automatic system would obtain more reliable input, thus reducing the interference with system control.

To further validate the confidence level of the planned trajectory relative to the human driver's lane-changing trajectory and the applicability of the algorithm to other human drivers, a third human driver C was randomly selected from the remaining 18 human drivers for planning and trajectory prediction verification in this section.

Figs. 12(a)–12(c) show the lane-changing trajectories and lane-changing features of human driver C under five clusters of vehicle velocities, respectively. Figs. 12(d) and 12(e) show the planned trajectories of human driver C for scenarios 1 and 2 at 10 and 15 $m{\cdot}s^{-1}$ velocities, respectively. In Figs. 12(f) and 12(g), the planned trajectories are placed under the trajectory clusters collected in the experiments. The results in Figs. 12(f) and 12(g) are the same as those in Figs. 11(b), 11(d), 11(f), and 11(h). The lane-changing time of human driver C is 5.0046 and 4.1552 s, respectively, which are 0.1114 and 0.0173 s different from the mean lane-changing time collected by human driver C, and the relative differences are 2.18% and 0.41%. As the variances of the mean lane-changing time of human driver C are 0.57, 0.37, 0.36, 0.34, and 0.20 s, the planned trajectories are within one-time variance. The planned trajectories are used to represent the lane-changing trajectory to be executed by the primary vehicle with a high degree of reliability. This is a fitting method based on the historical information, and the planned trajectory could be highly fitted to the real trajectory clusters and thus be regarded as the prediction result for the next lane-changing.

5.3 Trajectory verification based on single view angle driver model

In order to verify the feasibility of planned trajectories in the tracking control layer of intelligent vehicles, this paper develops a single-view driver model for trajectory tracking verification using the Simulink/CarSim co-simulation platform. In order to ensure the reliability of longitudinal velocity tracking, the longitudinal velocity is simply controlled. The main vehicle parameters in the procedure are shown in Table 4, and the results are shown in Fig. 13.

Fig. 13(a) shows the position error of six trajectories. The error range of six trajectories is (0, 0.051 m), which is consistent with the requirement of trajectory tracking. Fig. 13(b) shows the lateral acceleration of the six trajectories. The lateral acceleration range of the six trajectories is (−0.28 g, 0.27 g), which does not exceed the stability constraint of 0.4 g. Figs. 13(c) and 13(d) show the trajectories of human drivers A, B, and C at 10 and 15 $m{\cdot}s^{-1}$, respectively. The results show that the planned trajectory with current driver personality features could meet the requirements of vehicle execution under the condition of guaranteed stability and absolute safety.

6 Human-machine shared driving verification of human-like trajectory planning

In order to validate the potential of the planned human-like lane-changing trajectory to reduce human-machine conflict in the HMSD, the driving simulator shown in Fig. 2 is used for the HMSD driver-in-the-loop test in this section. The input of the HMSD is the sum of the input of the human driver and machine, the reference target of the steering system is the planned human-like lane-changing trajectory, and the controller is a single view angle driver model. The workbench is operated in real-time at 100 Hz.

Firstly, in order to provide a non-human-like lane-changing trajectory for comparison, the human-like indicator in Eq. (24) is deleted, leaving only the lane-changing efficiency indicator and smoothness indicator. With the sum of the above two indicators as the target income, comparative lane-changing trajectories are generated following the trajectory planning process in Fig. 1. In order to eliminate the interference of road curvature on the experimental results, the two planned trajectories are transformed to FCS, and the shared driving driver-in-the-loop experiments of corresponding drivers are carried out, respectively. The testers are informed in advance that the driving system is an HMSD system and that the automatic steering system would assist in the lane-changing. The testers could operate and input as his/her own needs. 20 human drivers have participated in the driver-in-the-loop test, and the HMSD results of human drivers A, B, and C, corresponding to Section 3.1, are selected for presentation and analysis. After the experiments, drivers' shared driving subjective feelings are interviewed and recorded as an auxiliary evaluation indicator. The HMSD results of drivers A, B, and C at 10 or 15 $m{\cdot}s^{-1}$ are shown in Fig. 14.

Fig. 14(a) shows the shared driving results of human driver A under the human-like lane-changing trajectory and non-human-like lane-changing trajectory proposed in this paper. When the human-like lane-changing trajectory is the target of the automatic steering system, the shared driving trajectory conforms the target trajectory. The shared driving trajectory is slightly delayed when the non-human-like lane-changing trajectory is the target. Fig. 14(b) shows the steering input angle of human driver A in two kinds of shared driving. When the human-like lane-changing trajectory is the goal of the automatic steering system, the steering input angle of human driver A is in the same direction as the shared driving trajectory. When the non-human-like lane-changing trajectory is the target, the steering input angle of human driver A is in the same direction of the shared driving trajectory within 10 m in the early stage of the lane-changing. However, the steering input angle of human driver A is opposite to the direction of the shared driving trajectory at the later stage of the lane-changing. Fig. 14(c) shows the shared driving results of human driver B under the human-like lane-changing trajectory and non-human-like lane-changing trajectory proposed in this paper. When the human-like lane-changing trajectory is the target of the

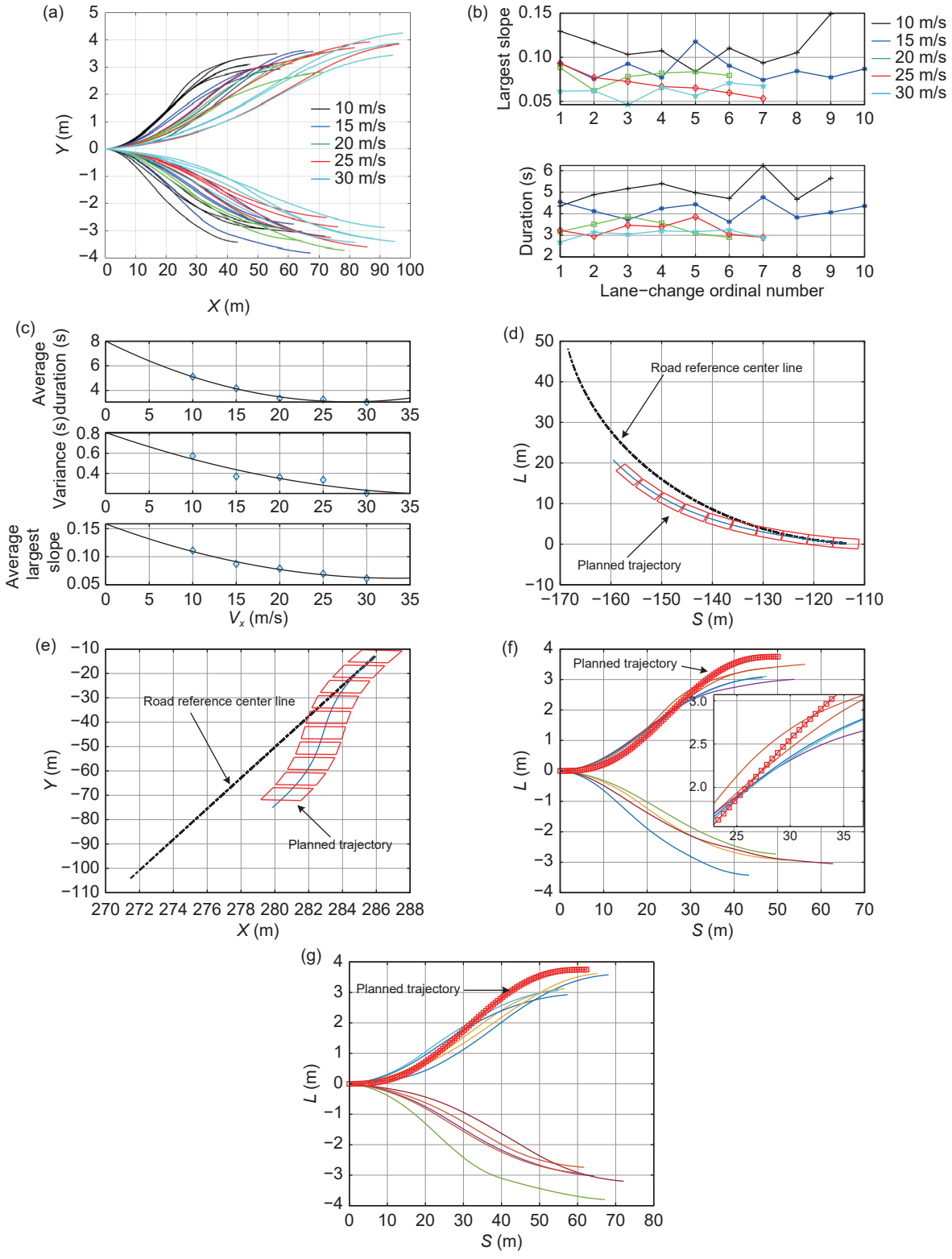

Fig. 12 (a) Intercepted lane-changing trajectory of human driver C at five clusters of vehicle velocities; (b) main lane-changing features of human driver C at five clusters of vehicle velocities; (c) main feature values of human driver C corresponding to the whole velocity range; (d) the planned trajectory of human driver C at 10 m·s^{-1} in scenario 1; (e) the planned trajectory of human driver C at 15 m·s^{-1} in scenario 2; (f) the planned trajectory and the lane-changing trajectory clusters of human driver C at 10 m·s^{-1}; (g) the planned trajectory and the lane-changing trajectory clusters of human driver C at 15 m·s^{-1}.

automatic steering system, the shared driving trajectory fits the target trajectory. When the non-human-like lane-changing trajectory is the target, the shared driving trajectory is delayed to the human-like lane-changing trajectory and has a long lane-changing end adjustment stage. Fig. 14(d) shows the steering input angle of human driver B for both shared driving trajectories, which behaves in the same way as Fig. 14(b).

Figs. 14(e) and 14(g) show the HMSD trajectory of human driver C at 10 and 15 m·s^{-1}, respectively. The performance of Figs. 14(e) and 14(g) are similar to that of driver A and driver B in

Table 4 Simulation parameters

Symbol	Interpretation	Value (unit)
m	Total mass	1,300 (kg)
I_Z	Moment of inertia	1,523 (kg·m^2)
l_f	Front axle distance	1.5 (m)
l_r	Rear axle distance	1.275 (m)
i	Steering ratio	16.7
T	Model discretized step	0.001 (s)
c_{max}	Coefficient	0.024
c_{min}	Coefficient	0.015

Figs. 14(a) and 14(c). Figs. 14(g) and 14(h) show the steering angle input of human driver C at 10 and 15 m·s^{-1}, respectively. The performance of Figs. 14(g) and 14(h) are similar to that of driver A and driver B in Fig. 14(b) and 14(d).

The results of shared driving trajectories in Figs. 14(a), 14(c), 14(e), and 14(g) show that human drivers still adhere to their own objectives in the process of shared driving lane-changing, and the trajectories are reflected as a more human-like lane-changing trajectory. The steering input angle of the human driver in Figs. 14(b), 14(d), 14(f), and 14(h) indicate that the human driver would be more likely to accept the trajectory like their own objective in the process of shared driving lane change, to form mutual assistance between the two sides. However, when the objective of the automatic steering system is significantly different from that of the human driver, resulting in the discomfort of the human driver, the human driver chooses the reverse input to offset the input of the automatic steering system. This would make the vehicle trajectory tend to the psychological expectations of human drivers. This process is the human-machine conflict stage. Figs. 14(b), 14(d), 14(f), and 14(h) show that the human-like lane-changing trajectory in this paper could reduce the occurrence of human-machine conflict.

The subjective driving experience of human driver A recorded that in the shared driving test with the human-like lane-changing trajectory, the lane-changing performances are like his own operation, and driver A could feel the driving assistance; in the shared driving test with a non-human-like lane-changing trajectory, the actual lane-changing operation performs urgently which would increase the driver's driving anxiety under the driving condition. The subjective driving experience of human driver B recorded that in the shared driving test with a human-like lane-changing trajectory, the lane change operations perform closely; in the shared driving test with a non-human-like lane-changing trajectory, compared with the previous one, the actual lane change operation performs faster. The subjective driving experience of human driver C recorded that in the shared driving test with a human-like lane-changing trajectory, driver C could feel noticeable driving assistance and lower steering interference on driver C's own driving operations; in the shared driving test with a non-human-like lane-changing trajectory, compared with the previous one, driver C could feel rapid changes in vehicle status and increased driving anxiety during multiple tests. In addition, driver C could feel the irregular torque fluctuation disturbance from the EPS system, which could provide more interference in the driver's manoeuvres.

Following the test, the test drivers are asked to subjectively choose their preferred lane-changing trajectory. 18 of 20 human drivers chose the human-like lane-changing trajectory, and the remaining 2 of 20 indicated that both trajectories are acceptable.

The experimental results demonstrate that the human-like lane-changing trajectory proposed in this paper greatly benefits in mitigating human-machine conflict in the HMSD systems. This would further enhance the trust and acceptance of human drivers to the HMSD system, reduce the possibility of human drivers competing for the right of the road with the automatic systems, and thus improve the safety of the HMSD system.

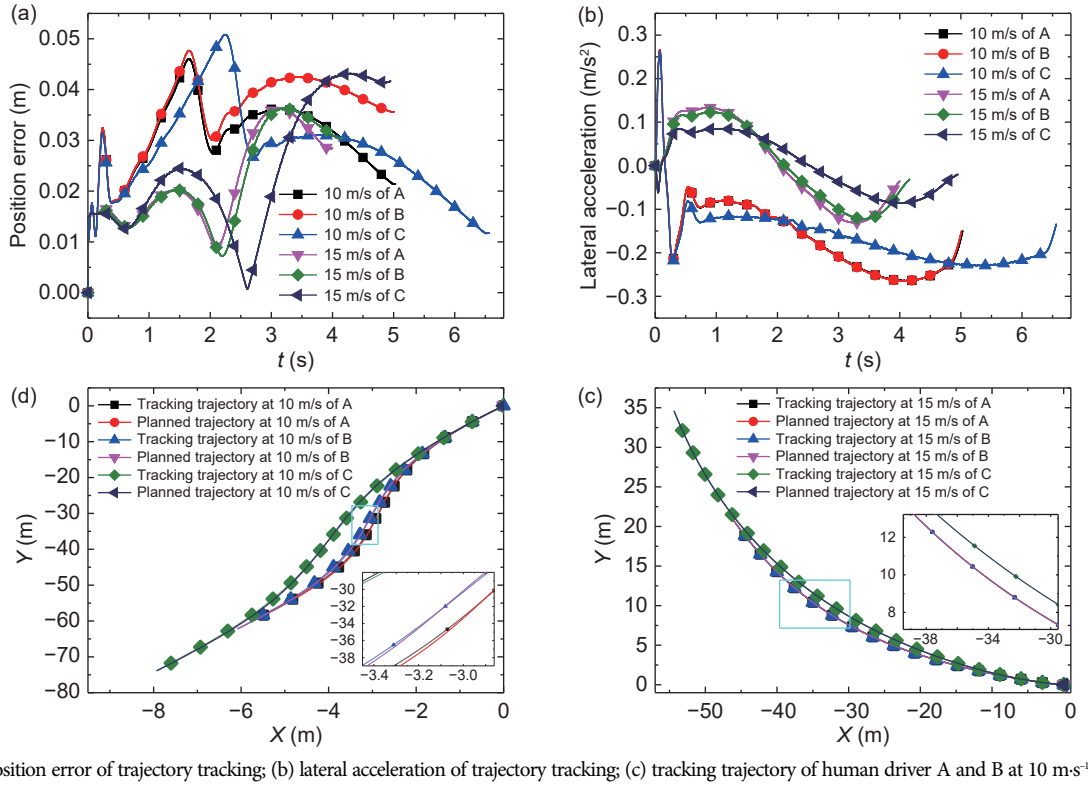

Fig. 13 (a) Position error of trajectory tracking; (b) lateral acceleration of trajectory tracking; (c) tracking trajectory of human driver A and B at 10 m·s^{-1} in scenario 1; (d) tracking trajectory of human driver A and B at 15 m·s^{-1} in scenario 2.

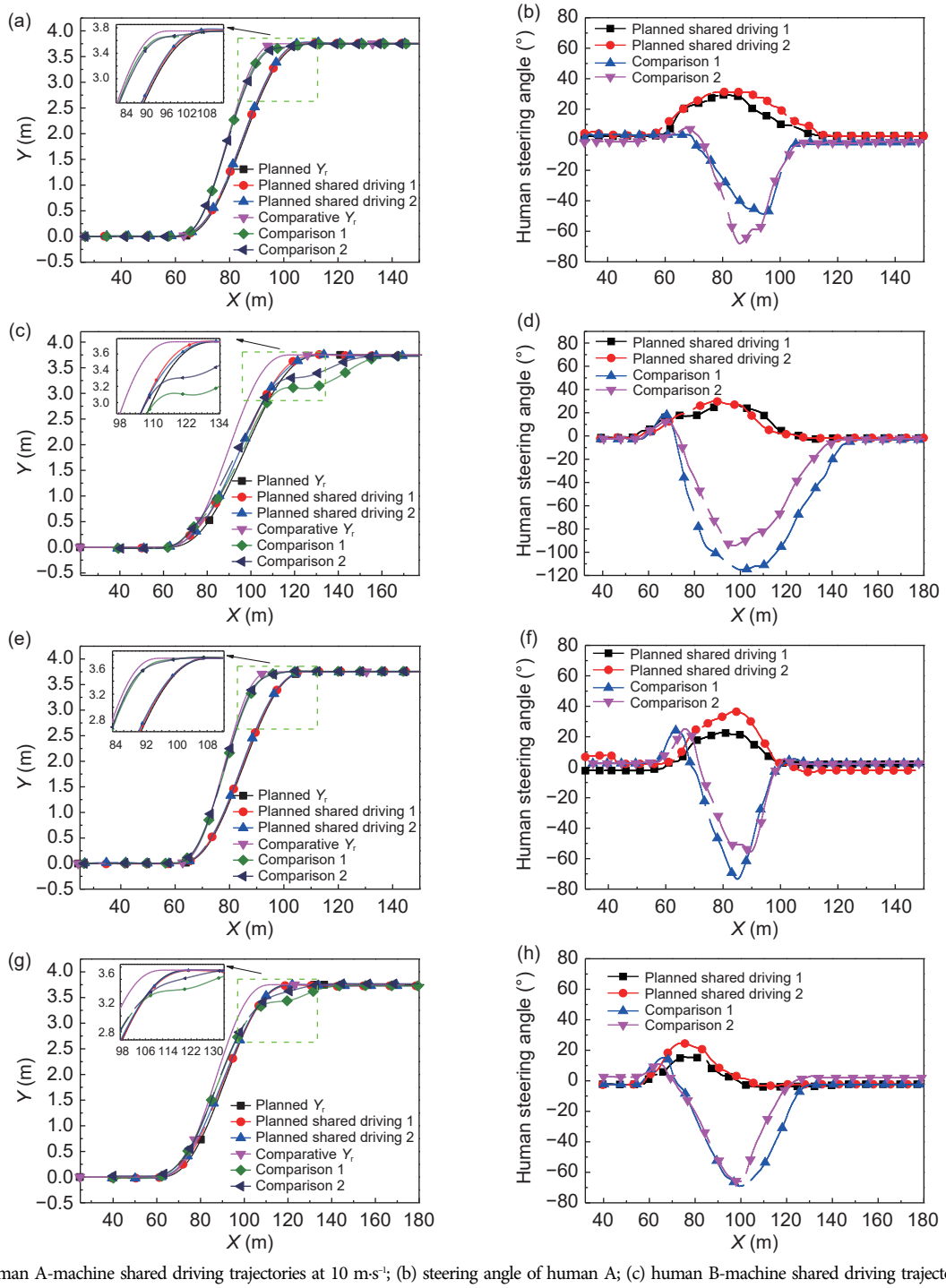

Fig. 14 (a) Human A-machine shared driving trajectories at 10 m·s^{-1}; (b) steering angle of human A; (c) human B-machine shared driving trajectories at 15 m·s^{-1}; (d) steering angle of human B; (e) human C-machine shared driving trajectories at 10 m·s^{-1}; (f) steering angle of human C; (g) human C-machine shared driving trajectories at 15 m·s^{-1}; (h) steering angle of human C.

7 Conclusions

This paper proposes a human-like lane-changing trajectory planning algorithm to mitigate the potential conflicts between the human drivers and the automation systems from the path planning level for autonomous driving cars. Firstly, a basic lane-changing trajectory algorithm based on the quintic polynomial in the FCS is developed. Following this, naturalistic driving data is collected in order to bring the planned trajectory closer to human behaviour, and based on which some lane-changing features are selected and analyzed. The human-like lane-changing trajectory considers vehicle dynamic stability performance, driving cost optimization, and collision avoidance. Finally, the single view angle driver model and the HMSD driver-in-the-loop test verify the proposed human-like trajectory tracking performance. Hence, we can draw the following conclusions from this paper:

1) The proposed vertex embedding collision avoidance algorithm could be efficiently employed in vehicle trajectory planning with collision detection and avoidance.

2) The proposed lane-changing trajectory planning algorithm with the highest degree of personalization provides a cluster of lane-changing trajectories that are highly compatible with human driving behaviour, and thus could further mitigate the potential driving conflict between human driver and automation systems.

3) The proposed trajectory planning algorithm's search method could reduce the planned trajectory's computation cost compared with other search algorithms.

4) The planned trajectory which highly fits the real lane-changing trajectory clusters could be further employed as an empirical human driver trajectory prediction result. The potential application of the proposed algorithm could be further extended for the research in the human driver trajectory prediction area.

It is worth noting that the trajectory planning algorithm proposed in this paper is based on lane-changing decisions to make actions, which may lead to no solution for the trajectory planning algorithm if the decisions are faulty in terms of environmental perception or velocity mismatch curvature. The lane-changing trajectory planning algorithm also has some application limitations and requires information on historical human driver behaviors. However, there are no implications for the application of this algorithm in the areas of human-machine conflict reduction and human-like driving assistance.

Acknowledgements

We sincerely thank the participants of our user study for their testing and the insightful comments they provided. This work is supported by Open Fund of State Key Laboratory of Automobile Simulation and Control of Jilin University (20201111).

Declaration of competing interest

Declaration of competing interest The authors have no competing interests to declare that are relevant to the content of this article.

References

Ali, Y., Zheng, Z., Haque, M. M., 2021. Modelling lane-changing execution behaviour in a connected environment: A grouped random parameters with heterogeneity-in-means approach. Commun Transport Res, 1, 100009.

Cao, T., Xiang, Z. Y., Liu, J. L., 2015. Perception in disparity: An efficient navigation framework for autonomous vehicles with stereo cameras. IEEE Trans Intell Transp Syst, 16, 2935–2948.

Chae, S. H., Kang, M. C., Sun, J. Y., Kim, B. S., Ko, S. J., 2017. Collision detection method using image segmentation for the visually impaired. IEEE Trans Consumer Electron, 63, 392–400.

He, X., Xu, D., Zhao, H., Moze, M., Aioun, F., Guillemard, F., 2018. A human-like trajectory planning method by learning from naturalistic driving data. In: 2018 IEEE Intelligent Vehicles Symposium (IV). June 26–30, 2018, Changshu, China. IEEE, 339–346.

Huang, C., Hang, P., Hu, Z., Lv, C., 2021. Collision-probability-aware human-machine cooperative planning for safe automated driving. IEEE Trans Veh Technol, 70, 9752–9763.

Kim, N., Cha, S., Peng, H., 2011. Optimal control of hybrid electric vehicles based on Pontryagin's minimum principle. IEEE Trans Control Syst Technol, 19, 1279–1287.

Kim, W., Son, Y. S., Chung, C. C., 2016. Torque-overlay-based robust steering wheel angle control of electrical power steering for a lane-keeping system of automated vehicles. IEEE Trans Veh Technol, 65, 4379–4392.

Li, B., Acarman, T., Peng, X., Zhang, Y., Bian, X., Kong, Q., 2020. Maneuver planning for automatic parking with safe travel corridors: A numerical optimal control approach. In: 2020 European Control Conference (ECC). May 12-15, 2020, St. Petersburg, Russia. IEEE, 1993–1998.

Li, M., Song, X., Cao, H., Wang, J., Huang, Y., Hu, C., *et al*., 2019. Shared control with a novel dynamic authority allocation strategy based on game theory and driving safety field. Mech Syst Signal Process, 124, 199–216.

Na, X., Cole, D. J., 2013. Linear quadratic game and non-cooperative predictive methods for potential application to modelling driver–AFS interactive steering control. Veh Syst Dyn, 51, 165–198.

Peng, T., Liu, X. L., Fang, R., Zhang, R. H., Pang, Y. W., *et al*., 2020. Lane-change path planning and control method for self-driving articulated trucks. J Intell Connect Veh, 3, 49–66.

Qi, X., Wu, G., Boriboonsomsin, K., Barth, M. J., 2017. Development and evaluation of an evolutionary algorithm-based onLine energy management system for plug-in hybrid electric vehicles. IEEE Trans Intell Transp Syst, 18, 2181–2191.

Russell, H. E. B., Harbott, L. K., Nisky, I., Pan, S., Okamura, A. M., Gerdes, J. C., 2016. Motor learning affects car-to-driver handover in automated vehicles. Sci Robot, 1, eaah5682.

Sun,B., 2020. Research on human-like shared control considering driver's driving capability and style. Ph.D. Dissertation. Changchun: Jilin University. (in Chinese)

Tan, D., Liu, S., Li, R., Yang, K., 2019. Research status of behaviour decision-making for intelligent vehicles. Int J Veh Inf Commun Syst, 4, 279.

Vigue, Y., Lichten, S. M., Blewitt, G., Heflin, M. B., Malla, R. P., 1992. Precise determination of Earth's center of mass using measurements from the global positioning system. Geophys Res Lett, 19, 1487–1490.

Wang, J., Zhang, Q., Zhang, Z., Yan, X., 2016. Structured trajectory planning of collision-free lane change using the vehicle-driver integration data. Sci China Technol Sci, 59, 825–831.

Werling, M., Kammel, S., Ziegler, J., Gröll, L., 2012. Optimal trajectories for time-critical street scenarios using discretized terminal manifolds. Int J Robotics Res, 31, 346–359.

Wu, J., Qu, X., 2022. Intersection control with connected and automated vehicles: A review. J Intell Connect Veh, 5, 260–269.

Xue, W., Zheng, R., Yang, B., Wang, Z., Kaizuka, T., Nakano, K., 2019. An adaptive model predictive approach for automated vehicle control in fallback procedure based on virtual vehicle scheme. J Intell Connect Veh, 2, 67–77.

Xu, S., Peng, H., 2019. Design, analysis, and experiments of preview path tracking control for autonomous vehicles. IEEE Trans Intell Transp Syst, 21, 48–58.

Xu, S., Peng, H., Tang, Y., 2020. Preview path tracking control with delay compensation for autonomous vehicles. IEEE Trans Intell Transp Syst, 22, 2979–2989.

Yan, C., Xie, H., Yang, D., Yin, J., Zhang, Y., Dai, Q., 2018. Supervised hash coding with deep neural network for environment perception of intelligent vehicles. IEEE Trans Intell Transp Syst, 19, 284–295.

Yang, Y., 2009. Chinese geodetic coordinate system 2000. Sci Bull, 54, 2714–2721.

Yuan, Y., Zhang, J., 2020. A novel initiative braking system with nondegraded fallback level for ADAS and autonomous driving. IEEE Trans Ind Electron, 67, 4360–4370.

Zhang, C., Chu, D., Lyu, N., Wu, C., 2019. Trajectory planning and tracking for autonomous vehicle considering human driver personality. In: 2019 3rd Conference on Vehicle Control and Intelligence (CVCI). September 21–22, 2019, Hefei, China. IEEE, 1–6.

Zhang, Q., Yang, X. J., Robert, L. P. Jr., 2021. Individual differences and expectations of automated vehicles. Int J Human–Computer Interact, 38, 825–836.

Zhao, B., Xu, N., Chen, H., Guo, K., Huang, Y., 2019. Stability control of electric vehicles with in-wheel motors by considering tire slip energy. Mech Syst Signal Process, 118, 340–359.

Zheng, H., Zhou, J., Shao, Q., Wang, Y., 2019. Investigation of a longitudinal and lateral lane-changing motion planning model for intelligent vehicles in dynamical driving environments. IEEE Access, 7, 44783–44802.

Zheng, L., Zeng, P., Yang, W., Li, Y., Zhan, Z., 2020. Bézier curve-based trajectory planning for autonomous vehicles with collision avoidance. IET Intell Transp Syst, 14, 1882–1891.

Zhou, J., Zheng, H., Wang, J., Wang, Y., Zhang, B., Shao, Q., 2019a. Multiobjective optimization of lane-changing strategy for intelligent vehicles in complex driving environments. IEEE Trans Veh Technol, 69, 1291–1308.

Zhou, Y., Cholette, M. E., Bhaskar, A., Chung, E., 2019b. Optimal vehicle trajectory planning with control constraints and recursive implementation for automated on-ramp merging. IEEE Trans Intell Transp Syst, 20, 3409–3420.

Zhu, B., Yan, S., Zhao, J., Deng, W., 2018. Personalized lane-change assistance system with driver behavior identification. IEEE Trans Veh Technol, 67, 10293–10306.

Changhua Dai received the B.S. degree from Jilin University, Changchun, China, in 2018. He is currently a Ph.D. student at the School of Automotive Engineering, Jilin University, China. His research interests include automotive dynamics simulation and control.

Changfu Zong received the B.S. degree from Liaoning University of Technology, Jinzhou, China, in 1986, the M.E. degree from Jilin University of Technology, Changchun, China, in 1994, and the Ph.D. degree from Jilin University of Technology, Changchun, China, in 1998. He is currently a Professor at the State Key Laboratory of Automotive Simulation and Control, Jilin University, Changchun. He has been an Academic Visitor at the University of Cambridge, UK, in 2005 and Senior Academic Visitor at the University of California, Berkeley, USA, in 2013. He has published over 200 articles. His research interests include vehicle control stability, new energy vehicle, intelligent networked vehicle control, and autonomous vehicle control.

Dong Zhang received the M.Sc. degree from Jilin University, Changchun, China, in 2015, and the Ph.D. degree from University of Lincoln, Lincoln, UK, in 2019. He is currently a Lecturer in the Department of Mechanical and Aerospace Engineering, Brunel University London, UK. He joined Brunel in 2021, having previously spent one year as a research fellow in the School of Mechanical and Aerospace Engineering and the School of Electrical and Electronic Engineering at Nanyang Technological University, Singapore. He has been with Brunel University since September 2021 and founded the Intelligent Driving and Transportation Research Group. He has published more than 30 articles in international journals as well as numerous conference articles, and about 10 granted patents mostly in the area of intelligent driving and transportation control and active safety systems for road vehicles.

Gang Li received the M.Sc. degree in vehicle engineering from Liaoning University of Technology, Jinzhou, China, in 2006, and the Ph.D. degree from Jilin University, Changchun, China, in 2013. He is currently a Professor and Dean of the School of Automobile and Traffic Engineering, Liaoning University of Technology, Jinzhou, China. He has authored or co-authored more than 50 journal and conference papers, and owns 30 China patents and software copyrights. His current research interests include modelling, simulation, intelligent control of vehicles, and vehicle active safety.

Kaku Chuyo received the M.Sc. degree in automotive engineering from Jilin University, Changchun, China, in 1988 and the Ph.D. degree in mechanical engineering from Tokyo Institute of Technology, Tokyo, Japan, in 1998. He is currently working for Jiangsu Chaoli Electric Co., Ltd., as Head of Chian as well as being the Director of the Technical Center and Chief Technical Manager. He was an Associate Professor at the Department of Automotive Engineering, Harbin Institute of Technology, Harbin, China, from 1988 to 2005. From 1998 to 2016, he had worked in engineering field at Hino Motor Co., Ltd., Siemens Automotive Japan, Toyota Motor Co., Ltd., Bosch Japan. He has been working on the chassis dynamics control projects over 30 years, and achieved more than 20 paper publications and patent certifications.

Hongyu Zheng received the B.S. degree in mechanical engineering and automation and the Ph.D. degree in vehicle engineering from Jilin University, Changchun, China, in 2003 and 2009, respectively. From October 2017 to October 2018, he was a Visiting Research Scholar at the Department of Mechanical and Aerospace Engineering, The Ohio State University, Columbus, OH, USA. He is currently a Professor at the State Key Laboratory of Automotive Simulation and Control, Jilin University. His research interests include vehicle dynamics and control as well as control of autonomous vehicles.

Fei Gao received the B.S. and Ph.D. degrees in automotive engineering from Jilin University, Changchun, China, in 2011 and 2017, respectively. From 2014 to 2015, she was a Visiting Scholar in Berkeley, California, USA. She is currently an Associate Professor at the State Key Laboratory of Automotive Simulation and Control Automotive Engineering in Jilin University and holds 4 patents. Her research interests include automotive human engineering and motion sickness.